observations of the CPE-complex on the plasma membrane and molecular structure of the full-length CPE.

Here, we describe the structure of CPE solved by X-ray crystallography at a resolution of 2.0 Å. Our results show that CPE shares features in common with aerolysin, *C. perfringens* ε-toxin, and *Laetiporus sulphureus* hemolytic pore-forming lectin, implying that CPE organizes transmembrane pores via the similar mechanism adopted by these toxins.

EXPERIMENTAL PROCEDURES

Plasmid construction- The CPE gene was amplified by PCR with the following primer pair: NcoCPE 5'-aaaaccatggcgATGCTTAGTAACAATTTAAAT C-3' (including a *Nco* I site (underlined)) and CPEXho 5'-aaactcgagAAATTTTTGAAATAATATTGAATAA -3' (including a *Xho* I site (underlined)) using pET16b-CPE (15) as the template. The amplified DNA fragment was cloned into pCR2.1-TOPO TA (Life Technologies Corp., Carlsbad, CA), and sequenced. The CPE gene with the correct sequence was excised with *Nco* I and *Xho* I and inserted into the *Nco* I-*Xho* I site of pET28a(+) (Merck KGaA, Darmstadt, Germany), so that the gene was fused to a hexahistidine-tag sequence on the 3' side. The resultant plasmid was named pET28a-CPEwt.

Expression and purification of CPE- Ten milliliters of an overnight culture of *E. coli* BL21-CodonPlus (DE3)-RIL (Stratagene, La Jolla, CA) transformed with pET28a-CPEwt was inoculated into 1 L of LB medium containing 50 μg/ml kanamycin and 50 μg/ml chloramphenicol. The culture was grown at 37°C with vigorous shaking until the absorbance at 600 nm reached 0.6. Expression of the recombinant protein was induced by adding isopropyl-1-thio-β-D-galactopyranoside (Nacalai tesque, Kyoto, Japan) to give a final concentration of 1 mM. Six hours later, the cells were harvested by centrifugation at 5,000 rpm for 20 min at 4°C, washed with ice-cold water, suspended in 50 mM Na-phosphate buffer, pH 8.0 including 0.3 M NaCl and 1 mM imidazole, and disrupted by sonication using Sonifier S-350 (Branson, Danbury, CT) at 4°C. The suspension of the disrupted cells was centrifuged at 12,000 rpm for 20 min at 4°C. The supernatant was subjected to nickel-NTA affinity gel (HIS-Select Nickel Affinity Gel, Sigma-Aldrich, St. Louis, MI) chromatography, and the soluble recombinant protein was eluted with an imidazole concentration gradient (1 - 500 mM). The fraction containing CPE was collected and dialyzed against 10 mM Tris-HCl pH 8.0. The homogeneity of the purified preparation was confirmed by 12.5 % PAGE without SDS.

Crystallization- An 8 mg/ml solution of the recombinant C-terminally His-tagged CPE in 0.01 M Tris-HCl pH 8.0 was employed for crystallization. Crystallization trials were set up at room temperature as sitting-drop vapor-diffusion experiments on Linbro crystallization plates. Initial screening was performed using the sparse-matrix method (Jancarik & Kim, 1991) with commercial crystal screening kits (Hampton Research). The crystallization droplets were made of 1 μl of the CPE solution and 1 μl of a reservoir solution containing 25% (w/v) polyethylene glycol 3350, 0.2 M sodium chloride and 0.1 M Tris-HCl, pH 8.0, at 293 K, and equilibrated with 500 μl of the reservoir solution. Triangle-shaped tabular crystals appeared in a few weeks and grew to maximum dimensions of about 0.3 × 0.3 × 0.2 mm.

Data collection, phasing and refinement- X-ray diffraction data on CPE crystals were collected at 100 K in a nitrogen stream, after the crystals were soaked with the reservoir solution containing 20% glycerol as a cryoprotectant. Native data at 1.98 Å were collected from a single crystal with a Rayonix MX225HE CCD detector on the beamline BL44XU at SPring-8 (Table 1). The X-ray wavelength was 0.9 Å, the angle oscillation range was 0.5° and the crystal-to-detector distance was 230 mm.

More than ten heavy-atom compounds were tested to collect diffraction data. Suitable derivatives were used such as $SmCl_2$ (soaking concentration, 5 mM), which yielded an overall figure of merit of 0.66 at 3.1 Å by a combination of single anomalous dispersion (SAD) and molecular replacement (MR) phasing (Table 1). Crystallographic phases were calculated and refined by *Phaser* (24). The resulting electron density maps modified by *Parrot* (25) automatically allowed the tracing of about 80% of one independent molecule by *Buccaneer* (26). Model building and inspection were based on *Coot* (27). Atomic coordinates and structural factors for CPE have been deposited with the Protein Data Bank, with accession code 3AM2. All images of the molecular structure were prepared with PyMol (http://www.pymol.org/).

RESULTS

Structural determination- The crystal data are shown in Table 1. Analysis of the diffraction pattern and systematic absences led to the CPE crystals being assigned to the cubic space group $P2_13$, with unit-cell parameters $a = b = c =$

98.5 Å, α = β = γ = 90°. A total of 22,192 unique reflections were obtained using the program packages of *HKL2000* (28). The intensity data in the resolution range of 69.6 to 1.98 Å were processed with an *R*-merge value of 6.9%. Assuming a molecular weight of 35 kDa for the expressed CPE, packing density calculations indicate the most probable value for V_M to be 2.27 $Å^3$ Da^{-1}, with one CPE chain per asymmetric unit. This corresponds to a solvent fraction of about 45.9 %, a typical value for protein crystals.

The crystal structure of the full-length CPE was solved by a combination of SAD methods using samarium derivatives and MR techniques with the Lys^{197} to Phe^{319} region of C-CPE (PDB accession code 2QUO). The experimental maps calculated by the *Phaser* and *Parrot / Bucaneer* procedures were of excellent quality and allowed unequivocal tracing of the chain (residues 36-319), and subsequent refinement at a resolution of 1.98 Å. The structure was refined using *REFMAC* (29); 5% of the unique reflections were used to monitor the free *R*-factor. The final values for the general *R*-factor and free *R*-factor were 19.3% and 25.2%, respectively (all reflections in the 69.6-1.98 Å range). The refined model consists of 286 amino acids with 136 solvent molecules and two unknown ions. Stereochemistry checks indicated that the refined model was in quite good agreement with expectations for models within this resolution range (Table 1). For N-terminal residues 1–35, electron density was not observed, implying a disordered structure. The asymmetric unit contained one CPE molecule (Fig. 1), and its trimers were generated by crystallographic symmetry (Fig. 2).

CPE monomer- The monomer of CPE shows an elongated shape (95 x 42 x 32 Å), which is composed of 17 β strands and 5 helices, three of which are very short, comprising less than 6 amino acid residues (Fig. 1). These results are consistent with previous data from circular dichroism spectra showing that CPE contains about 80% β sheet (30). Three distinct domains could be distinguished in the molecule and were designated domain I, domain II, and domain III as shown in Fig. 1. Domain I almost corresponds to the region referred to as C-CPE, which binds to the specific receptor claudin (2,4). This domain forms a nine-strand β sandwich with a short helical element between strands β9 and β10, the fold of which is almost the same as that reported previously (14), except for some loop regions (residues 217-223 and 265-272). The crystal packing is, however, completely different. The major interactions in the previously determined structure mainly involve Arg^{227} and Ser^{304}, whereas in the structure determined here, marked hydrophobic interactions occur between Val^{282} in the C-terminal region, and Phe^{319} in the C-terminal region of a neighboring molecule (31). Domains II and III organize a module, which shows an elongated caterpillar shape, 60 Å long and 24–28 Å thick (Fig. 1). The module is composed of 8 β-sheets, β1 to β8, two α helices, and two short 3_{10} helical segments. Two long β-strands, β6 and β7, organize a stem which spans the entire length of the module with a slight distortion between the domains. In addition, domain II contains the largest α-helix, and three β-strands that form an antiparallel sheet together with β6 and β7. Domain III contains three β-strands and three small helices in addition to β6 and β7.

Trimeric assembly of CPE- Although the monomer of CPE is found in the asymmetric unit in this crystal, it does form a crystallographic trimer (Fig. 2, A and B). The trimeric fold is stabilized by a number of specific interactions between each monomer. Analyses with PISA (http://www.ebi.ac.uk/msd-srv/prot_int/pistart.html) revealed major interactions between domain III and domain I of two symmetry-related molecules. The helical regions at the edges of domain III interact with the β-barrel region of domain I of an adjacent molecule. Arg^{208} of domain I is inserted into α2, which has negatively charged interfaces (Fig. 2C). On the other side, Phe^{268} of the loop connecting β13 and β14 of domain I is hydrophobically inserted into helix 3_{10}b at the edge of domain III (Fig. 2D). These two specific interactions determine the position of domain I relative to domain III. The trimeric assembly shows an apparent conduit structure in its center. Glu^{94} and Glu^{110} face the respective counterpart of each monomer and organize the narrow regions (diameter = 4.4-4.6 Å) of the conduit (Fig. 2E). Although the α1 helices of each monomer are close to each other, directed toward the conduit, there are neither α helices nor β sheets forming the conduit walls. Analysis of samarium-derivative data sets shows that three symmetrical side chains of Glu^{94} and Glu^{110} keep a samarium ion in each narrow region. To know whether the conduit structure is involved in the toxicity of CPE, we examined CPE mutants, in which Glu^{94} or Glu^{110} was independently replaced with Asp, Gly, Gln, Tyr, or Leu, for cytotoxicity in Vero cells. All the CPE mutants were found to retain the cytotoxicity (data not shown).

Structural homologues of CPE- A DALI search (http://ekhidna.biocenter.helsinki.fi/dali_server/start) for structural homologues of the full-length CPE uncovered a hemagglutinin component, HA3, of *C.*

botulinum toxin, and *C. perfringens* ε-toxin. *C. botulinum* HA3 is expressed as a single chain and proteolytically cleaved into HA3a and HA3b chains, both of which share homology with the N-terminal module of CPE composed of domains II and III (2ZOE-A chain, Z = 14.0; 2ZOE-B chain, Z = 10.9). BLAST also revealed the amino-acid sequences of HA3a (residues 17-173, genebank ID D38562) and HA3b (residues 211-423, genebank ID D38562) to show 24% and 27% identity with CPE, residues 33-188 and 39-240, respectively. In contrast to HA3, the structural similarity of *C. perfringens* ε-toxin with CPE is low (1UYJ, Z = 5.2). When domains II and III of CPE were subjected to the DALI search, aerolysin and *Laetiporus sulphureus* hemolytic pore-forming lectin (LSL) also emerged in addition to *C. perfringens* ε-toxin (Fig. 3A).

DISCUSSION

The pore-forming toxins exert their toxic effects by elaborating physiological pores on the plasma membrane of target cells, resulting in changes to the membrane's permeability and eventually cell lysis. These toxins are divided into two groups, α -pore-forming toxins (α-PFTs) and β-pore-forming toxins (β-PFTs), based on structural properties of transmembrane pores. The former group employs α -helices to insert into the lipid membrane, and the latter uses β -strands to fold amphipathic β -barrels in the membrane (32,33). *Salmonella* cytolysin A and staphylococcal δ-toxin exemplify the former (23,32), and many other pore-forming toxins belong to the latter. Although CPE has long been believed to be a pore-forming toxin, the architecture of the pore it creates has been unknown. Briggs et al. reported the preliminary crystallographic data of CPE but did not described the details (31). In this study, we first determined the overall structure of CPE, information which then enabled us to speculate on the mechanism by which it forms pores.

The structure of CPE provided several points of note. First, CPE shows a trimeric form with an apparent conduit/channel in crystal packing, with which may suggest a physiological channel made by CPE as a pore-forming toxin. However, it is unlikely that this conduit functions as actual transmembrane pores for the following reasons. 1) Unlike in the case of other PFTs, the conduit is not surrounded by a rigid structure such as an α helix or β barrel. 2) The vertical size of the trimer containing the conduit is estimated at 52 Å at most, which is not enough to span the lipid bilayer membrane. 3) In gel permeation chromatography, CPE eluted at a position estimated at 35 kDa, indicating the toxin to be in a monomeric state in solution (data not shown). In addition, there have been no reports to show that CPE is oligomerized in solution. 4) Glu^{94} and Glu^{110} face the respective counterpart of each monomer and organize the narrow points in the conduit (Fig. 2E). This structure implies these residues are critical in the function of any pores organized by the trimer. However, substitutions of these residues with Asp, Gln, Gly, Tyr, or Leu did not affect the toxicity (data not shown). 5) The conduit is organized above the receptor-binding site, which is located at the bottom of domain I in the trimeric state shown in Fig. 2B. Therefore, the conduit should be positioned above the plasma membrane surface and is not able to make a transmembrane pore. 6) Asp^{48}, which was reported to be important in the oligomerization of the toxin (7), is located outside of the interface of the trimer (Fig. 2A). These findings indicate that the trimeric assembly with the conduit-like structure emerges only in the crystal.

Second, the CPE monomer shares structural homology with *C. botulinum* HA3 and *C. perfringens* ε-toxin, which also show structural homology between each other. HA3 is a component of a hemagglutinin and known to bind to sialyl-oligosaccharides (34). However, because the sugar-binding ability is attributable to a region of HA3 that is not homologous to CPE, it is difficult to predict the structure-function relation of CPE, based on the homology with HA3. Instead, we focus on characteristic features of CPE that are common among the pore-forming toxins such as *C. perfringens* ε-toxin, aerolysin and LSL. These toxins have an elongated architecture with β sheets and an arrangement of three (or four) domains (17,35,36)(Fig. 3A). In this study, the domains of CPE were numbered after those of the other toxins: Domains I, II and III (Figs 1 and 3). Domain I is composed of the C-terminal region of CPE whereas domains II and III are formed by the N-terminal region. As a result, the amino acid sequence and the domain arrangement of CPE were in the opposite order, whereas *C. perfringens* ε-toxin, aerolysin and LSL consist of domains I, II, III (and IV for aerolysin) from the N- to C- terminus.

As shown in Fig. 3A, these domains are aligned along the long axis of the toxins, except domain I of aerolysin. Domain I (or domains I and II of aerolysin) is responsible for binding to respective receptors. Aerolysin is known to bind a certain set of glycosylphosphatidylinositol-anchored proteins. Domain I of LSL is defined as a lectin binding to

carbohydorates. The receptor for ε toxin is not known. Although these toxins similarly have the receptor-binding site/residues at the top (Fig. 3A, red sticks), they show less structural similarity in domain I than other domains. It is plausible that the distinct structure of domain I (and domain II for aerolysin) reflects the different receptors recognized by these domains. In contrast to domain I, the module composed of domains II and III shares several structural features in common with these toxins, notably in terms of the stem of two β strands and a flanking element laying on the major β-sheet in domain II (or domain III for aerolysin) (Fig. 3A, yellow ribbons). The flanking element of CPE shows alternating patterns of polar and hydrophobic residues, which imply amphipathic characteristics. Amphipathic strands have been found in similar flanking elements of aerolysin (16), *C. perfringens* ε-toxin (35), LSL (36), staphylococcal α toxin (21) and leukocidin (37) (Fig. 3B), all of which are known as β -PFTs. Biochemical analyses of *C. septicum* α-toxin, which shows clear homology with aerolysin, identified the membrane-spanning domain as an amphipathic region corresponding to the flanking region of aerolysin (38). These strands are believed to be inserted into the lipid bilayer and form the transmembrane β-barrel, the hydrophobic residues of which face the lipid bilayer and the polar residues of which constitute the hydrophilic lumen of pores (Fig. 3C). The amphipathic strand of CPE stretches from Val^{81} to Ile^{106}, and comprises β4, α1, and the intervening loop (Figs. 1 and 3). A previous report demonstrated that this region participates in the formation of pores after organizing a pre-pore oligomeric complex (7). Taken together, it is likely that CPE belongs to the β-PFT family, and the Val^{81}-Ile^{106} region forms the β-hairpin to organize the β-barrel structure spanning the lipid membrane (Fig. 3C).

The amphipathic flanking strands reside in the middle of the toxin molecule. Therefore, if this strand takes part in the formation of the transmembrane pore, a certain structural alteration of the toxin must occur. Previous reports demonstrate that cholesterol-dependent cytolysins, a group of β-PFTs including perfringolysin O and pneumolysin, undergo vertical collapse that brings the amphipathic strand to the membrane surface and forms the membrane pore composed of the β-barrel (19,39). We consider that similar structural changes occur for CPE to accomplish the β-barrel's insertion into the membrane. The cholesterol-dependent cytolysins consist of four domains, of which domain 2 is considered to be folded over bringing the amphipathic strand close enough to the membrane to span the bilayer. Domain 2 of cholesterol-dependent cytolysins and domains II and III of CPE possess at least two long antiparallel β-strands (Fig. 4A, orange strands). Thus, we presume that CPE, like the cholesterol-dependent cytolysins, inserts the amphipathic strand from β4 to α1 into the membrane upon the buckling of domains II and III, which may be conducted by the long antiparallel β-strands as a "hinge module" (Fig. 4B). This mechanism might be applicable to aerolysin, *C. perfringens* ε-toxin, and LSL, because they also have similar long antiparallel β-strands.

Here, we presented an explanation of how CPE forms a transmembrane pore, based on observations of the structural features of the full-length toxin. CPE is considered to be a β-PFT. The amphipathic region from Val^{81} to Ile^{106} is inserted into the plasma membrane upon the buckling of the stem module, a mechanism which may be common among some β-PFTs. To test our hypothesis, we are now trying to determine the structure of a CPE-claudin complex or an oligomerized form of CPE, which would enable us to better understand the pore-forming mechanism.

REFERENCES

1. Sonoda, N., Furuse, M., Sasaki, H., Yonemura, S., Katahira, J., Horiguchi, Y., and Tsukita, S. (1999) *J Cell Biol* **147**, 195-204
2. Katahira, J., Inoue, N., Horiguchi, Y., Matsuda, M., and Sugimoto, N. (1997) *J. Cell Biol.* **136**, 1239-1247
3. Hanna, P., Mietzner, T., Schoolnik, G., and McClane, B. (1991) *J Biol Chem* **266**, 11037-11043
4. Horiguchi, Y., Akai, T., and Sakaguchi, G. (1987) *Infect Immun* **55**, 2912-2915
5. Kokai-Kun, J. F., Benton, K., Wieckowski, E. U., and McClane, B. A. (1999) *Infect Immun* **67**, 5634-5641
6. Smedley, J. G., 3rd, and McClane, B. A. (2004) *Infect Immun* **72**, 6914-6923

7. Smedley, J. G., 3rd, Uzal, F. A., and McClane, B. A. (2007) *Infect Immun* **75**, 2381-2390
8. Robertson, S. L., Smedley, J. G., Singh, U., Chakrabarti, G., Van Itallie, C. M., Anderson, J. M., and McClane, B. A. (2007) *Cell Microbiol* **9**, 2734-2755
9. Takahashi, A., Kondoh, M., Masuyama, A., Fujii, M., Mizuguchi, H., Horiguchi, Y., and Watanabe, Y. (2005) *J Control Release* **108**, 56-62
10. Kondoh, M., Masuyama, A., Takahashi, A., Asano, N., Mizuguchi, H., Koizumi, N., Fujii, M., Hayakawa, T., Horiguchi, Y., and Watanbe, Y. (2005) *Mol Pharmacol* **67**, 749-756
11. Takahashi, A., Komiya, E., Kakutani, H., Yoshida, T., Fujii, M., Horiguchi, Y., Mizuguchi, H., Tsutsumi, Y., Tsunoda, S., Koizumi, N., Isoda, K., Yagi, K., Watanabe, Y., and Kondoh, M. (2008) *Biochem Pharmacol* **75**, 1639-1648
12. Harada, M., Kondoh, M., Ebihara, C., Takahashi, A., Komiya, E., Fujii, M., Mizuguchi, H., Tsunoda, S., Horiguchi, Y., Yagi, K., and Watanabe, Y. (2007) *Biochem Pharmacol* **73**, 206-214
13. Ebihara, C., Kondoh, M., Harada, M., Fujii, M., Mizuguchi, H., Tsunoda, S., Horiguchi, Y., Yagi, K., and Watanabe, Y. (2007) *Biochem Pharmacol* **73**, 824-830
14. Van Itallie, C. M., Betts, L., Smedley, J. G., McClane, B. A., and Anderson, J. M. (2008) *J Biol Chem* **283**, 268-274
15. Kimura, J., Abe, H., Kamitani, S., Toshima, H., Fukui, A., Miyake, M., Kamata, Y., Sugita-Konishi, Y., Yamamoto, S., and Horiguchi, Y. (2010) *J. Biol. Chem.* **285**, 401-408
16. Iacovache, I., Paumard, P., Scheib, H., Lesieur, C., Sakai, N., Matile, S., Parker, M. W., and van der Goot, F. G. (2006) *EMBO J* **25**, 457-466
17. Parker, M. W., Buckley, J. T., Postma, J. P., Tucker, A. D., Leonard, K., Pattus, F., and Tsernoglou, D. (1994) *Nature* **367**, 292-295
18. Wilmsen, H. U., Leonard, K. R., Tichelaar, W., Buckley, J. T., and Pattus, F. (1992) *EMBO J* **11**, 2457-2463
19. Czajkowsky, D. M., Hotze, E. M., Shao, Z., and Tweten, R. K. (2004) *EMBO J* **23**, 3206-3215
20. Sekiya, K., Danbara, H., Yase, K., and Futaesaku, Y. (1996) *J Bacteriol* **178**, 6998-7002
21. Song, L., Hobaugh, M. R., Shustak, C., Cheley, S., Bayley, H., and Gouaux, J. E. (1996) *Science* **274**, 1859-1866
22. Dutta, S., Mazumdar, B., Banerjee, K. K., and Ghosh, A. N. (2010) *J Bacteriol* **192**, 169-178
23. Mueller, M., Grauschopf, U., Maier, T., Glockshuber, R., and Ban, N. (2009) *Nature* **459**, 726-730
24. McCoy, A. J., Grosse-Kunstleve, R. W., Adams, P. D., Winn, M. D., Storoni, L. C., and Read, R. J. (2007) *J Appl Crystallogr* **40**, 658-674
25. Cowtan, K. (2010) *Acta Crystallographica Section D Biological Crystallography* **66**, 470-478
26. Cowtan, K. (2008) *Acta Crystallogr D Biol Crystallogr* **64**, 83-89
27. Emsley, P., and Cowtan, K. (2004) *Acta Crystallogr D Biol Crystallogr* **60**, 2126-2132
28. Otsinoski, Z., and Minor, W. (1997) *Methods Enzymol* **276**, 307-326
29. Murshudov, G. N., Vagin, A. A., and Dodson, E. J. (1997) *Acta Crystallogr D Biol Crystallogr* **53**, 240-255
30. Granum, P. E., and Harbitz, O. (1985) *J. Food Biochem.* **9**, 137-146
31. Briggs, D. C., Smedley, J. G., McClane, B. A., and Basak, A. K. (2010) *Acta Crystallogr F Struct Biol Cryst Commun* **66**, 794-797
32. Geny, B., and Popoff, M. R. (2006) *Biol Cell* **98**, 667-678
33. Gouaux, E. (1997) *Curr Opin Struct Biol* **7**, 566-573
34. Nakamura, T., Kotani, M., Tonozuka, T., Ide, A., Oguma, K., and Nishikawa, A. (2009) *Journal of Molecular Biology* **385**, 1193-1206
35. Cole, A. R., Gibert, M., Popoff, M., Moss, D. S., Titball, R. W., and Basak, A. K. (2004) *Nat Struct Mol Biol* **11**, 797-798
36. Mancheño, J. M., Tateno, H., Goldstein, I. J., Martínez-Ripoll, M., and Hermoso, J. A. (2005) *J Biol Chem* **280**, 17251-17259
37. Miles, G. (2002) *Protein Science* **11**, 894-902
38. Melton, J. A., Parker, M. W., Rossjohn, J., Buckley, J. T., and Tweten, R. K. (2004) *J Biol Chem* **279**, 14315-14322
39. Tilley, S. J., Orlova, E. V., Gilbert, R. J. C., Andrew, P. W., and Saibil, H. R. (2005) *Cell* **121**, 247-256
40. MacKenzie, C. R., Hirama, T., and Buckley, J. T. (1999) *J Biol Chem* **274**, 22604-22609

41. Rossjohn, J., Feil, S. C., McKinstry, W. J., Tsernoglou, D., van der Goot, G., Buckley, J. T., and Parker, M. W. (1998) *J Struct Biol* **121**, 92-100

FOOTNOTES

We thank Dr. K. Matoba and Prof. S. Harada of Kyoto Institute Technology, and Dr. E. Yamashita, Dr. Y. Umena and Prof. A. Nakagawa of SPring-8 BL44XU for their help with the X-ray data collection. Diffraction data were collected at the Osaka University beamline BL44XU at SPring-8 equipped with MX225-HE (Rayonix), which is financially supported by Academia Sinica and National Synchrotron Radiation Research Center (Taiwan, ROC). We also appreciate secretarial and technical assistance by Ms. T. Suzuki and Ms. M. Kobayashi. This work was supported in part by Grants-in-Aid for Scientific Research from the Ministry of Education, Culture, Science, and Technology of Japan.

FIGURE LEGENDS

Figure 1. Three-dimensional structure of the full-length CPE monomer. (A) Ribbon diagram of the CPE monomer. The N-terminal pore-forming domain II, domain III, and the C-terminal claudin-binding domain I are shown in blue, light pink, and lime green, respectively.
(B) Amino acid sequence and secondary structure of CPE. Arrows and end-rounded bars below the sequence indicate β-strand and helical conformations, respectively. Domains I, II, and III are represented by green, blue and magenta, respectively.

Figure 2. Trimeric structure of CPE. (A) View from the top of the trimer and parallel to the three-fold axis. (B) View perpendicular to the three-fold axis. Each monomer is defined by a different color, blue, green, or pink. Asp^{48} is rendered as red sticks in each monomer. (C-E) Views of the interface between monomers. Residues directly involved in contact between the monomers are shown as stick models. The calculations of interfaces between monomers were performed by PISA. (C and D) Dimeric interface between domains I and III. (E) Trimeric interfacing center of CPE. Glu^{94} and Glu^{110} of each monomer are featured as magenta and light blue sticks, respectively.

Figure 3. Structural similarities between aerolysin, *C. perfringens* ε-toxin, LSL, and CPE. (A) Ribbon diagrams are drawn from PDB data under accession codes, 1PRE for aerolysin (17), 1UYJ for *C. perfringens* ε-toxin (35), 1W3F for LSL (36) and, 3AM2 for CPE (this study). Domains corresponding to domains I, II, and III of CPE are defined by green, blue, and pink, respectively. Domains I and II of aerolysin are shown in green. Amphipathic loops (flanking elements) are indicated as yellow ribbons. The residues that participate in receptor binding are depicted as red sticks (11-13,15) (40) (36). Note that each toxin possesses at least two long antiparallel β-strands spanning domains II and III (domains III and IV for aerolysin). (B) Sequence alignment of the putative transmembrane domains of different β-PFTs; the aerolysin-like family, aerolysin

(Aer), ε-toxin (Epn), and LSL, three staphylococcal pore-forming toxins, *S. aureus* α-toxin (Hln, PDB code 7AHL), LukF (PDB code 1PVL), and LukS (PDB code 1T5R), and CPE. The numbers after the toxin names indicate the N-terminal amino acid positions. Alignments were generated based on the alternating pattern of polar and hydrophobic residues. Residues that are putatively facing the lipid bilayer are shown in blue. (C) Schematic representation of the antiparallel strands forming the β-barrel of staphylococcal α-toxin and the corresponding residues of CPE and aerolysin. The alignment is based on previous reports (21,37,41) and sequence similarity. The residues are portrayed as either facing the lipid bilayer or lining the lumen of the pore.

Figure 4.

Comparison of structure between CPE and perfringolysin O (PFO, accession code 1PFO) (A) and a putative model showing how the toxin molecules are folded to insert the antipathic strands into the membrane (B). Each domain of CPE is represented by the same colors as shown in Fig. 3A. (A) The long antiparallel strands are shown in orange. (B) The diagram was drawn based on a model presented previously (39). The long antiparallel strands that function as a hinge module are shown as an orange bar. 1: Binding to the membrane surface via domain I (DI). 2: The prepore complex shown with three monomers. 3: The amphipathic strand is inserted upon the buckling of the module composed of domains II and III.

Table 1. Data collection, structural solution, and refinement statistics for CPEs

Diffraction data	CPE	
	Native1	$SmCl_2$
X-ray source	SPring-8 /BL44XU	CuKα
Wavelength (Å)	0.900	1.54178
Resolution (Å)	1.98	3.1
Space gruop	$P2_13$	$P2_13$
Unique reflections	22192	6058
*R*merge (%)*	6.9(31.9)	12.0(48.8)
Completeness (%)[+]	99.3(100)	100(100)
Redundancy	10.5	21.3
Refinement	*Refmac5*	
Resolution range (Å)	69.6 - 1.98	
*R*factor*/*R*free* (%)	19.3/25.2	
No. of protein atoms	2236	
No. of solvent atoms	136	
Ramachandran distribution (% favoured, allowed, outlier)	98.0, 1.4, 0	
R.m.s. bonds (Å), angles (°)	0.023, 1.95	
Average B value (Å^2)	43.3	

* $R_{merge} = \Sigma | Ii - \langle Ii \rangle | / \Sigma \langle Ii \rangle$, where Ii is the observed intensity and $\langle Ii \rangle$ is the average intensity over symmetry equivalent measurements.

$R_{factor} = \Sigma | | Fobs | - | Fcalc | | / \Sigma | Fobs |$

R_{free} is calculated as R_{factor}, but on 5% of all reflections, that were not used in the crystallographic refinement.

[+] Completeness for all reflections and for the highest resolution shell in parentheses.

Fig. 1, Kitadokoro et al.

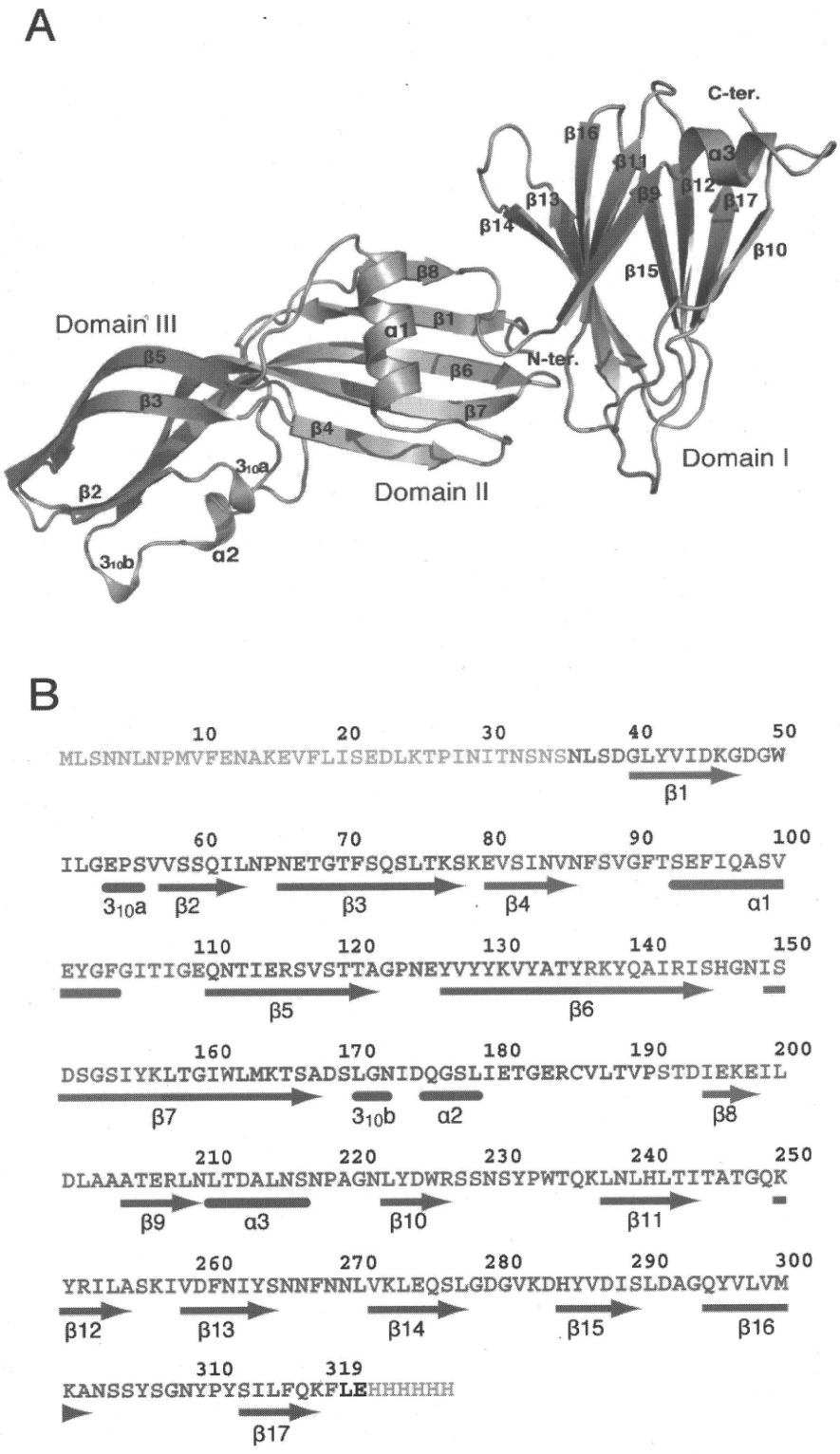

Fig. 2, Kitadokoro et al.

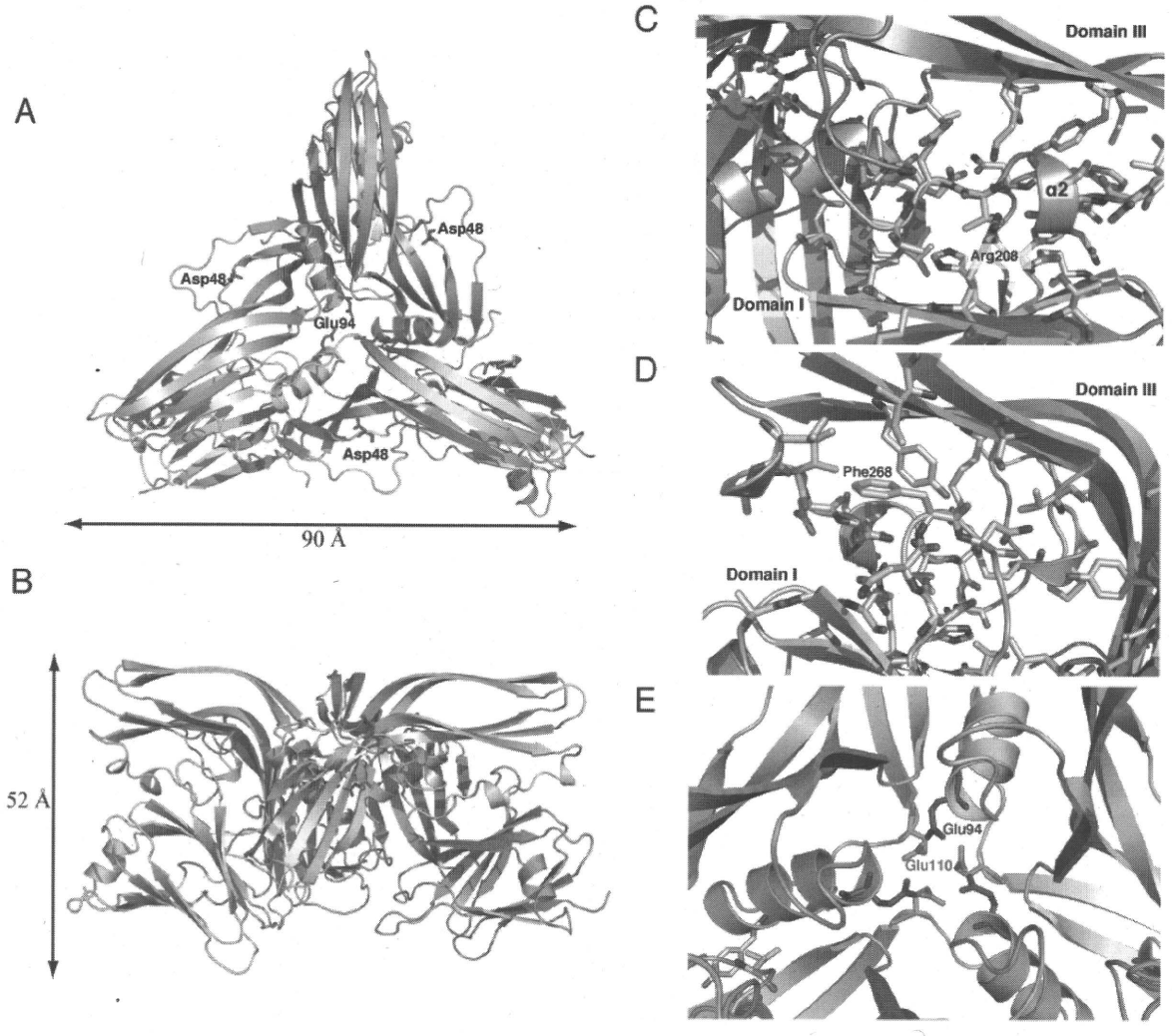

Fig. 3, Kitadokoro et. al

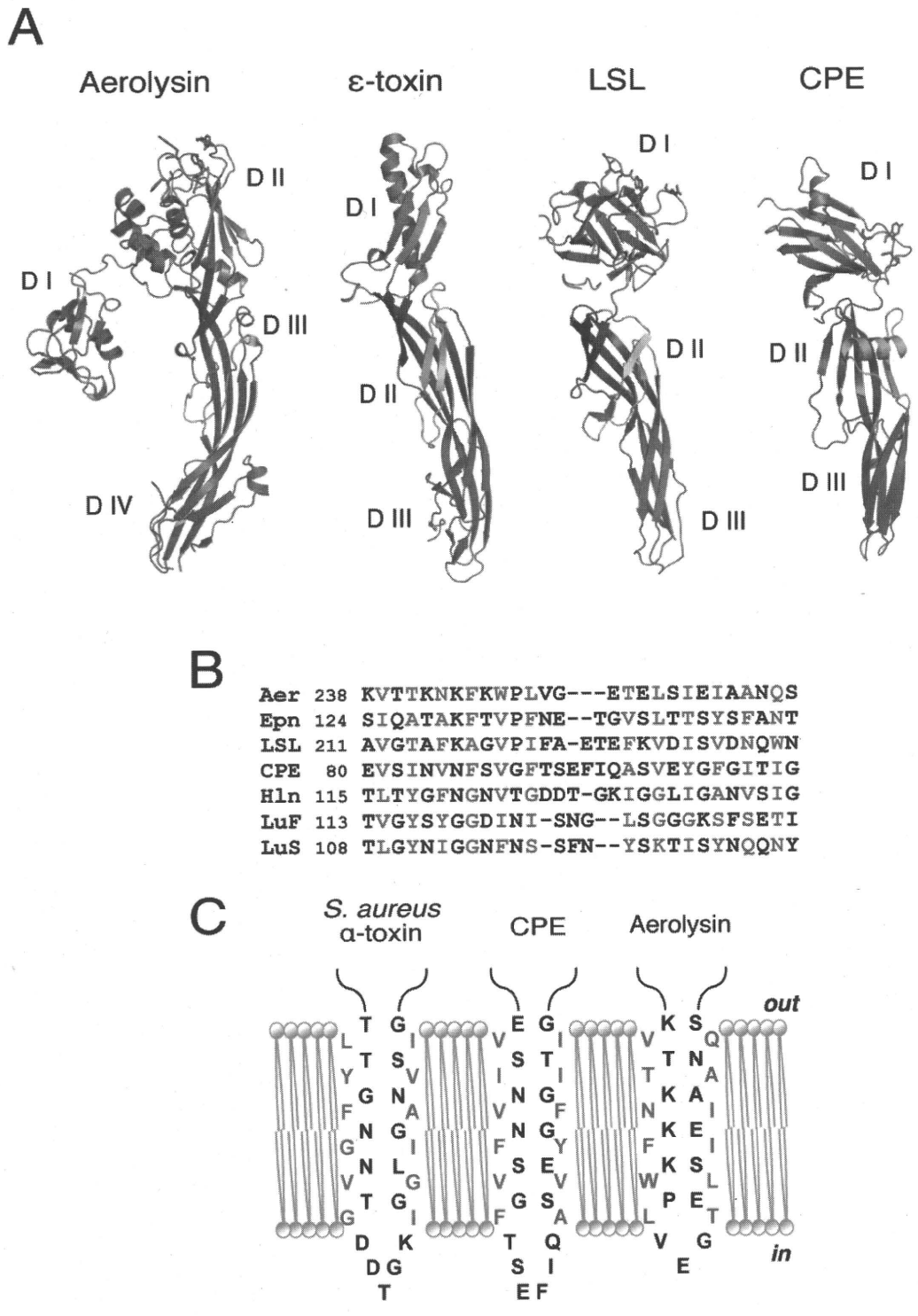

Fig. 4, Kitadokoro et. al.